Supporting Information for

Two-point optical manipulation reveals mechanosensitive remodeling of cell-cell contacts in vivo

Kenji Nishizawa, Shao-Zhen Lin, Claire Chardès, Jean-François Rupprecht, Pierre-François Lenne

Pierre-Francois Lenne E-mail: pierre-francois.lenne@univ-amu.fr,
Jean-François Rupprecht E-mail: jean-francois.rupprecht@univ-amu.fr

This PDF file includes:

Supporting Information Text

1. Experimental methods

A. Effects of laser power. Near-infrared femtosecond lasers can produce damage and temperature increase (1). In Bambarderkar et al (2), we monitored the cell response at different laser powers; we found that the amplitude of the junction deflection is proportional to the laser power ranging from 50 to 300 mW (deviations to the linear regime occurred above 300 mW).

To assess potential cell damage due to laser, we exposed cells to laser irradiation for 60 s at 200, 400 and 600 mW (Fig. S1 A), by focusing the laser in the center of cells (at the height of adherens junctions). At 200 and 400 mW, we did not observe any significant deformation. However, at 600 mW, we observed tissue contraction, indicative of damaging effects. We also tested the effects of static laser traps on junctions: we exposed single junctions for 60 s at 400 mW to a single laser focus (Fig. S1 B) and two junctions for 60 s at 200 mW with dual traps positioned in the middle of junctions like in the *diagonal push/pull* experiments (Fig. S1 C). In both cases, we did not observe any significant deformation within 60 s. We decided to use 200 mW per trap for manipulation, which induces sufficiently large deflections (when the traps are moved) without observable cellular damage.

In the two-trap experiments, the two traps are generally more than 5 μm apart (*diagonal pull/push*), and given the dissipation of heat in water, we do not expect that the temperature effects would be significantly different from those of single-point manipulation. A potential critical case is *direct push* manipulation, for which the two laser foci overlap for 60 s which leads to a local power exposure of 400 mW. To check that *direct push* is not a consequence of thermal effects, we repeated the experiments using 100 mW per laser trap and found that at this power, full junction shrinkage can also be achieved (Fig. S1 D).

B. Changes in the length of junctions a few cells away from the manipulation points. As a control, we monitored the length of junctions at a few cell distances (>5 and <10) from the points of manipulation and with the same orientation as the middle junction in the *diagonal pull* manipulation (Figure 1E (i) in main text). These junctions did not change significantly in length, as junctions without manipulation(Fig. S2).

C. Dextran injection. To detect potential large-size disruption of the junctions or changes in the axial position of cells during manipulation, we injected fluorescently labeled Dextran (10000 MW, -Alexa568, Cie) between the vitelline membrane and the apical surface of the epithelial tissue (Fig. S3). Dextran cannot enter cells but diffuses fast between them, thus marking the extracellular space. The laser spots are located at the adherens junction plane located at 1 μm distance from the apical surface. We did not detect any significant changes of Dextran signal at junctions during manipulation (Fig. S3 B). This observation rules out the possibility that changes in junction length are due to damage of the junctions or axial movement of the cells due to optical force application.

D. Changes in junction length after trap release. Tension dynamical remodeling manifests in the adaptation of tension to strains. Such adaptation is encapsulated in the rates of tension remodeling under contraction or extension, k_c and k_e respectively. A prediction of negative (or positive) k_c is that after a junction contraction, tension decreases (or increases). To verify this prediction, we performed *direct push* manipulation in conditions where Myosin-II mechanosensitive response was abolished (Rock inhibited tissues). In such conditions, *direct push* manipulation produces only partial shrinkage, and the vertices escape the optical traps short after manipulation (Fig. 4A). We measured the junction length after trap release and at the onset of manipulation (Fig. S4). Junction length was always found larger after trap release than at the onset of manipulation. Such extension suggests that the tension of the junction is decreased after contractile strain, which is consistent with $k_c < 0$.

2. Model methods

A. Vertex model motion equation. We use the vertex model to simulate the early *Drosophila* epithelium under local pulling/pushing forces applied by optical tweezers. In the vertex model, an epithelium cell sheet is described by a two-dimensional planar polygonal network where cells are represented by interconnected polygons. Cell–cell interfaces are traditionally characterized by straight lines which connect two neighboring tricellular junctions. Here, for the sake of mimicking pulling/pushing forces applied at the middle of some cell–cell interfaces, we divide each cell–cell interface into two segments, as shown in Fig. S6.

The dynamics of the epithelium is dictated by the force balance equation at each vertex i. Assuming pure frictional dynamics, the force balance equation reads:

$$\underbrace{\mathbf{F}_i^{(\mathrm{friction})}}_{\text{friction force}} + \underbrace{\mathbf{F}_i^{(\mathrm{passive})}}_{\text{internal passive force}} + \underbrace{\mathbf{F}_i^{(\mathrm{trap})}}_{\text{external pulling/pushing force}} = \mathbf{0}, \tag{1}$$

which accounts for a balance between the friction forces, the internal passive forces, and the external pulling/pushing forces. The first term represents the friction force between cells and the environment, which can be simply expressed as, $\mathbf{F}_i^{(\mathrm{friction})} = -\gamma \mathbf{v}_i$, with γ being the friction coefficient and $\mathbf{v}_i = \mathrm{d}\mathbf{r}_i/\mathrm{d}t$ being the velocity of vertex i. The second term is the internal passive forces stemming from a mechanical energy E such that $\mathbf{F}_i^{(\mathrm{passive})} = -\partial E/\partial \mathbf{r}_i$; while the third term refers to the external pulling/pushing force applied by the optical tweezers.

Trap force – To mimic the locally applied forces, we assume an elastic spring between the optical trap and the vertex under pulling/pushing. Assuming linear elasticity, the external pulling/pushing force can be written as

$$\mathbf{F}_i^{(\mathrm{trap})} = \begin{cases} K_{\mathrm{trap}}\left(\mathbf{r}_{i,\mathrm{trap}} - \mathbf{r}_i\right) & , \quad \text{if vertex } i \text{ is under pulling/pushing} \\ \mathbf{0} & , \quad \text{otherwise} \end{cases}, \tag{2}$$

where K_{trap} is the stiffness of the elastic spring connecting the optical trap and the vertex under pulling/pushing; $\mathbf{r}_{i,\mathrm{trap}}$ is the position of the optical trap that pulls or pushes vertex i.

Mechanical energy – We express the mechanical energy of a *Drosophila* epithelium as (3–6),

$$E = \underbrace{\sum_J \frac{1}{2} K_A (A_J - A_0)^2}_{\text{area elasticity}} + \underbrace{\sum_{\langle i,j \rangle} \Lambda_{ij} l_{ij}}_{\text{interfacial tension}}, \tag{3}$$

where the two terms account for the cell area elasticity and the cell–cell interfacial tension, respectively. K_A is the area stiffness of cells; A_J is the area of the $J-$th cell and A_0 is the preferred area. In addition, Λ_{ij} represents the dynamic interfacial tension (which remodels dynamically according to junction strain, see Eq. (4)) of the junction ij, and $l_{ij} = |\mathbf{r}_i - \mathbf{r}_j|$ is the junction length.

To mimic the heterogeneity of the cell–cell interfacial tension T_{ij}, before pulling/pushing perturbations ($t < 0$), we assume a Gaussian distribution of Λ_{ij}, $\Lambda_{ij} \sim \mathcal{N}(\mu_T, \sigma_T^2)$ with μ_T being the mean value and σ_T being the standard deviation.

Normalization – In simulations, we normalize the above governing equations using the length scale $\ell = \sqrt{A_0}$, the time scale $\tau = \gamma/(K_A A_0)$, and the stress scale $\sigma = K_A A_0$.

B. Junctional tension/strain remodeling. Here we consider a strain-dependent tension remodeling behavior of cell–cell junctions, following (7). Specifically, the cell–cell junction tension remodelling can be described by the following dynamic equation,

$$\frac{\mathrm{d}\Lambda_{ij}}{\mathrm{d}t} = \begin{cases} -k_{\mathrm{e}}\left(l_{ij} - l_{0,ij}\right) & \varepsilon_{ij} > \varepsilon_{\mathrm{cr}} \\ 0 & -\varepsilon_{\mathrm{cr}} < \varepsilon_{ij} < \varepsilon_{\mathrm{cr}} \\ -k_{\mathrm{c}}\left(l_{ij} - l_{0,jj}\right) & \varepsilon_{ij} < -\varepsilon_{\mathrm{cr}} \end{cases} \tag{4}$$

where k_{e} and k_{c} are the tension remodeling rates under junction extension or contraction, respectively; $\varepsilon_{ij} = (l_{ij} - l_{0,ij})/l_{0,ij}$ is the strain of the cell–cell junction ij with $l_{0,ij}$ being the rest length; $\varepsilon_{\mathrm{cr}}$ is a critical strain beyond which cell–cell junction tension remodeling is triggered.

Further assuming continuous strain relaxation of cell–cell junctions (7), the rest length $l_{0,ij}$ of the cell–cell junction ij evolves according to

$$\frac{1}{l_{0,ij}} \frac{\mathrm{d}l_{0,ij}}{\mathrm{d}t} = k_L \varepsilon_{ij}, \tag{5}$$

where $k_L > 0$ is the relaxation rate of rest cell–cell junction length $l_{0,ij}$ to the current cell–cell junction length l_{ij}. At steady state, we have $l_{ij} = l_{0,ij}$.

C. Myosin accumulation induced by junction shrinkage. The experimental results presented in the main text (Figure 4) reveal that myosin accumulation at cell–cell junctions is enhanced with large shrinking rates ($\dot{\varepsilon}_{ij} < \dot{\varepsilon}_{\rm cr}^{\rm (myo)} < 0$).

Inspired by this experimental observation, here we define the final model (called model D in the main text) where the Myosin–II accumulation induced tension $T_{ij}^{\rm (myo)}$ (along the junction between the vertices i and j) evolves according to the relation

$$T_{ij}^{\rm (myo)}(t) = T_m \int_{-\infty}^{t} \chi(t-\tau) f\left[\dot{\varepsilon}_{\rm cr}^{\rm (myo)} - \dot{\varepsilon}_{ij}(\tau)\right] {\rm d}\tau, \qquad [6]$$

where T_m is the tension magnitude induced by myosin accumulation; $\chi(t)$ is a memory kernel, which we will specify in the next paragraph; $f[\dot{\varepsilon}_{ij}]$ is the myosin activation function, which we model as:

$$\begin{aligned} f[\dot{\varepsilon}_{ij}] &= H\left[\dot{\varepsilon}_{\rm cr}^{\rm (myo)} - \Delta_\varepsilon - \dot{\varepsilon}_{ij}\right] + H\left[\dot{\varepsilon}_{\rm cr}^{\rm (myo)} - \dot{\varepsilon}_{ij}\right] H\left[\dot{\varepsilon}_{ij} - \dot{\varepsilon}_{\rm cr}^{\rm (myo)} + \Delta_\varepsilon\right] \left[\frac{\dot{\varepsilon}_{\rm cr}^{\rm (myo)} - \dot{\varepsilon}_{ij}}{\Delta_\varepsilon}\right]^\lambda, \\ &= \begin{cases} 0 & , \quad \dot{\varepsilon}_{ij} > \dot{\varepsilon}_{\rm cr}^{\rm (myo)}, \\ \left[\dfrac{\dot{\varepsilon}_{\rm cr}^{\rm (myo)} - \dot{\varepsilon}_{ij}}{\Delta_\varepsilon}\right]^\lambda & , \quad \dot{\varepsilon}_{\rm cr}^{\rm (myo)} - \Delta_\varepsilon < \dot{\varepsilon}_{ij} < \dot{\varepsilon}_{\rm cr}^{\rm (myo)}, \\ 1 & , \quad \dot{\varepsilon}_{ij} < \dot{\varepsilon}_{\rm cr}^{\rm (myo)} - \Delta_\varepsilon, \end{cases} \end{aligned} \qquad [7]$$

with an exponent $\lambda > 0$ and width $\Delta_\epsilon > 0$, which controls the smoothness of the activation function. In the limiting case $\lambda \to 0$ or $\Delta_\epsilon \to 0$, the activation function $f[\dot{\varepsilon}_{ij}]$ reduces to a step function; $\dot{\varepsilon}_{\rm cr}^{\rm (myo)}$ is a strain rate threshold.

In the next two paragraphs, we will consider two possible choices of the kernel function χ.

C.1. Exponential memory kernel. We first consider a standard memory kernel (8),

$$\chi(t-\tau) = \frac{1}{\tau_m} \exp\left(-\frac{t-\tau}{\tau_m}\right). \qquad [8]$$

with τ_m a characteristic time shift of the Myosin–II signal with respect to the strain-rate one.

The Myosin–II accumulation model of Eq. (8) can successfully lead to junctional shrinkage of the middle junction, as well as to the correct statistics for the neighbouring junctions (as in Fig. 4H) for a given set of parameters ($\tau_m = 50$ s, $T_m = 270$ pN, $\lambda = \Delta_\epsilon = 0$). However, the corresponding cumulative distribution function (CDF) of full-junction shrinkage time does not fit the experimental CDF; see Fig. S10. Indeed, the experimental CDF demonstrates a two-slope behavior and a broad distribution, ranging from ~ 10 s to ~ 100 s (see Fig. 4I in the main text). We further considered that the characteristic time τ_m could be Gaussian-distributed, yet the corresponding CDF still failed to match the one of experiments (Fig. S10(a)).

C.2. Gaussian kernel with a time-delay. To achieve a more quantitative fit of the cumulative distribution of the middle junction shrinkage time in the direct push case (see Fig. 4I in the main text), we consider a Gaussian kernel

$$\chi(t-\tau) = \frac{\sqrt{2}}{\tau_m\sqrt{\pi}} \exp\left[-\frac{1}{2}\left(\frac{t-\tau_d-\tau}{\tau_m}\right)^2\right], \qquad [9]$$

where τ_d and τ_m are a time delay and a time blur, respectively, of the Myosin–II signal with respect to the strain-rate one.

We define *Model D* by combining Eq. (9) with a distribution of time delays τ_d that corresponds to a Gaussian distribution that is truncated (i.e. conditioned) to positive values. We consider a distribution with mean value $\langle\tau_m\rangle = 54.2$ s and a standard deviation s.d.$(\tau_d) = 43.3$ s (these values are obtained after truncation of a Gaussian distribution with mean $\langle\tau_m\rangle = 50$ s and standard deviation s.d.$(\tau_d) = 50$ s). Last, we consider a sharp activation signal, with $\lambda = 0.1$.

The Model D, defined for this specific set of values, allows for a quantitative fit of the experimental CDF, see Fig. S11.

Narrower distribution of the time delay times (i.e. lower values of the standard deviation) or less sharp activation function (i.e. higher values of λ) increase the discrepancies with respect to the experimental CDF, see Fig. S11.

In addition, our simulations also suggest that the two-slope feature of the CDF of the middle junction full shrinkage time is not moderately sensitive to the value of the mean time delay $\langle\tau_d\rangle$, see Fig. S12.

D. Prediction on the effect of the laser power. We next evaluated the influence of the strength of the optical trap on the full shrinkage statistics.

In experiments, we lowered the power of the optical trap from 200 mW (control case) to 100 mW per trap for manipulation. As compared to the 200 mW case, fewer junctions shrunk completely, yet these showed lower shrinkage time (40 ± 34 s in the 200 mW against 34 ± 18 s in the 100 mW case, see Fig. S13(c)).

In simulations using Model D, the effect of the reduction in the laser intensity was accounted for by a two-fold decrease of the trap stiffness $K_{\rm trap}$, from 50 to 25 pN $\cdot\, \mu$m^{-1} As in experiments, fewer junctions shrunk completely, yet these showed lower shrinkage time, see Fig. S13(a, b).

These results suggest that the Myosin–II accumulation dominates the full shrinkage of the middle junction, both in simulations and experiments.

E. Estimation of the parameter values.

Area forces We measured the area of *Drosophila* epithelial cells as $A = 37.4 \pm 2.0\ \mu\text{m}^2$ (see Fig. S7(a)). Thus, assuming the incompressibility of cells, we can roughly take $A_0 = 36\ \mu\text{m}^2$, which leads to the length scale for our simulation system as $\ell = \sqrt{A_0} = 6\ \mu$m. Assuming the cell area stiffness $K_A = 10^6\ \text{N} \cdot \text{m}^{-3}$ (9), we then have the stress scale as $\sigma = K_A A_0 = 36\ \text{pN} \cdot \mu\text{m}^{-1}$.

Tension forces Previous experimental study measured that the tension T_{ij} is on the order of 44 ± 22 pN (2). We thus set the mean cell–cell interfacial tension as $\mu_T = \langle T_{ij} \rangle = 44$ pN.

Trap forces The stiffness of the spring connecting the optical trap and the vertex under pulling/pushing is taken as $K_{\text{trap}} = 50\ \text{pN} \cdot \mu\text{m}^{-1}$ to model the effect of the trapping by a laser at 200mW (2). Such value results in $\tilde{K}_{\text{trap}} = K_{\text{trap}}/(K_A A_0) \approx 1.39$. The displacement of the optical trap in experiments is $\Delta_{\text{trap}} \sim 1.2\ \mu$m, i.e. $\tilde{\Delta}_{\text{trap}} = \Delta_{\text{trap}}/\sqrt{A_0} \approx 0.2$.

Friction By comparing the time evolution of junction length between experiments and simulations, see Fig. 2C in the main text, we define the time scale as $\tau = \gamma/(K_A A_0) = 1\,\text{s}$.

Therefore, in our simulations, we set the values of dimensionless parameters as below: $\tilde{\mu}_T = 0.2$, $\tilde{\sigma}_T = 0.05$, $\tilde{K}_{\text{trap}} = 1.4$, $\tilde{\Delta}_{\text{trap}} = 0.2$, and $\Delta\tilde{t} = 0.01$ (see also Table S1).

Using such a parameter set, we have obtained a cellular pattern as shown in Fig. S6(b). We further compute the distribution of cell area, cell perimeter and cell shape index and compare them with experiments, as shown in Fig. S7. It demonstrates that for the epithelial pattern obtained from our simulations, the distributions of geometric properties of cells are similar to those of our experiments.

For the parameters involved in junctional tension/strain remodeling and Myosin–II accumulation (k_{L}, k_{e}, k_{c}, k_{m}, etc.), we have tested each in the parameter space and compare the junction elongations with our experimental measurements and set their values that best fit our experiments. For example, we represent in Fig. S9 how the middle junction elongation (*diagonal pull* case) varies with the parameter k_{e}; comparing them with our experiments, we set $k_{\text{e}} = 0.005$ ($= 0.18\ \text{pN} \cdot \mu\text{m}^{-1} \cdot \text{s}^{-1}$) in our present study unless stated otherwise.

F. Numerical procedure. Our simulation procedure is as follows:

1. We begin with a hexagonal cell pattern (see Fig. S6(a)) consisting of $N \approx 100$ cells in a periodic box $[0, L_x] \times [0, L_y]$, satisfying $L_x L_y = N A_0$, i.e. $\langle A_J \rangle_J = A_0$. We then randomly set the tension Λ_{ij} of each cell–cell junction ij, satisfying a Gaussian distribution, i.e. $\Lambda_{ij} \sim \mathcal{N}(\mu_T, \sigma_T^2)$. The system is relaxed to a steady state (see Fig. S6(b)), according to the motion equation Eq. (1) (mind that, at this stage, $\mathbf{F}_i^{(\text{trap})} = \mathbf{0}$ here). At each simulation time step, we estimate the new vertex position through a forward Euler scheme as $\mathbf{r}_i(t + \Delta t) = \mathbf{r}_i(t) + \mathbf{v}_i \Delta t$. T1 topological transitions are implemented any time the length threshold reaches the value $\tilde{\Delta}_{T1} = 0.01$ (i.e. $\Delta_{T1} = 0.06\ \mu$m).

2. Once we obtain the relaxed cell configuration (Fig. S6(b)), we randomly choose a short junction (with the length l_{ij} satisfying $0.9\ \mu\text{m} < l_{ij} < 2.4\ \mu$m, i.e. $0.15 < \tilde{l}_{ij} < 0.4$) of the tissue, which will correspond to the junction called middle junction in experiments (see the junction $C - D$ in Fig. S8).

3. We then add at $t = 0$ pulling/pushing forces to the vertices corresponding to the experimental setup of interest (see Fig. S8 for details). Specifically, we set the position of the associated optical trap acting on a vertex i as $\mathbf{r}_{i,\text{trap}}(t = 0) = \mathbf{r}_i(t = 0) + \Delta_{\text{trap}} \mathbf{t}_{i,\text{trap}}$ with Δ_{trap} being the displacement magnitude of the trap and $\mathbf{t}_{i,\text{trap}}$ being the pulling/pushing direction. We then fix the position of the optical trap $\mathbf{r}_{i,\text{trap}}(t) =$ constant and let the system evolve according to the motion equation Eq. (1).

3. Figures and Table

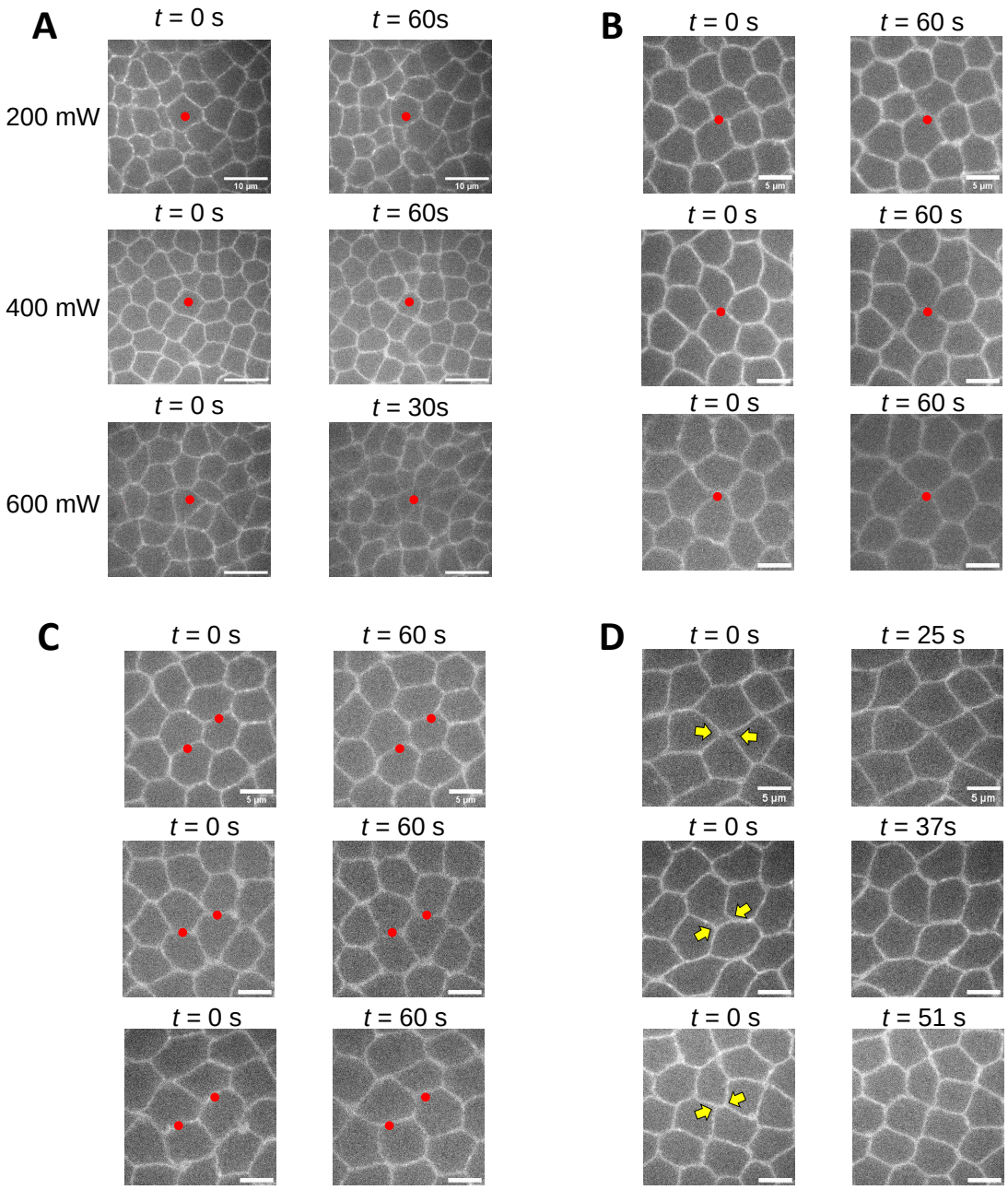

Fig. S1. Effects of laser power. (A) Effects of static laser traps on cells. We exposed cells to laser irradiation for 60 s at 200 mW (top), 400 mW (middle) and 30 s at 600 mW (bottom) by focusing the laser in the center of cells (at the height of adherens junctions). Red circles are the positions of laser focus. The cell junctions are labelled by Ecad::GFP. Scale bar: 10 μm. (n=5 per experiment). (B) Effects of static laser traps on junctions. We exposed cells to laser irradiation for 60 s at 400 mW by focusing the laser in the center of junctions. Scale bar: 5 μm. (n=6) (C) Two-point optical manipulation. We exposed cells to laser irradiation for 60 s at 200 mW per trap by focusing the laser in the center of junctions. Scale bar: 5 μm. (n=5). (D) *direct push* on vertices with 100 mW per trap. Scale bar: 5 μm. (n=6).

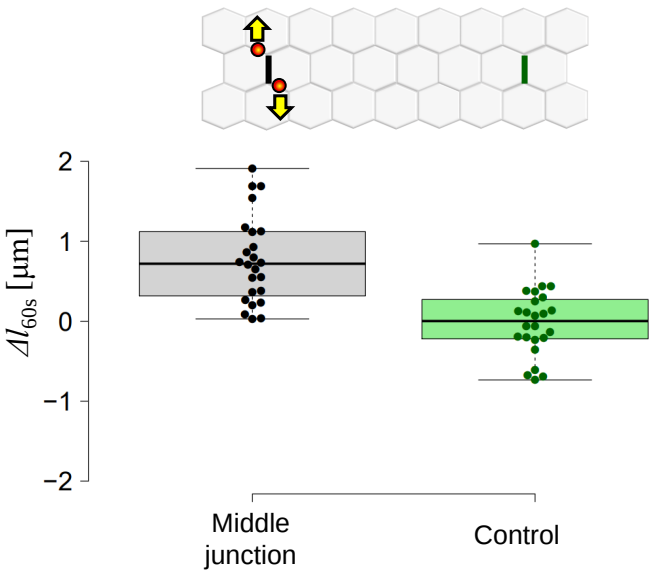

Fig. S2. Comparison of the length changes at 60 s post-manipulation ($diagonal\ pull$) of the middle junction (black points N=25, same data from Figure 1E (i)) and control, defined over junctions which are at a distance larger than 5 cells (and smaller than 10 cells) from the manipulated cells and with the same orientation as the middle junction (green points N=25 analyzed within the same image sequence as those used for analyzing the extension of the middle junction).

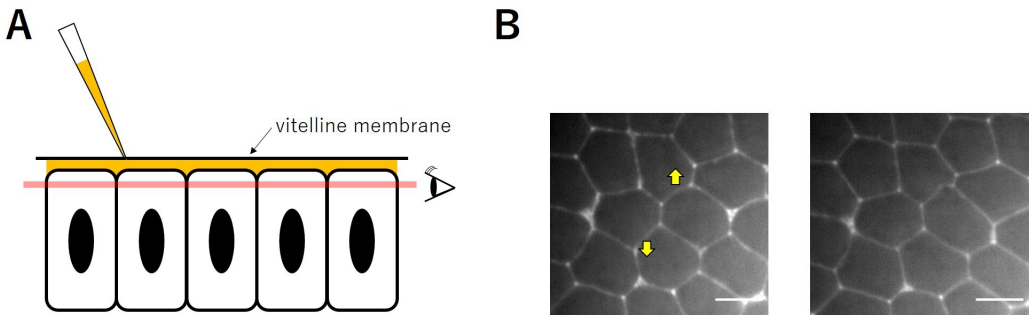

Fig. S3. (A) Fluorescently-labeled dextran solution is injected the perivitelline space. (B) The traps are moved away from each other, in antiparallel direction and maintained at 1 μm distance from their initial position (yellow arrows) causing junction remodeling. The right image shows the epithelial cells 1 minute after the onset of manipulation. Scale bar: 5 μm.

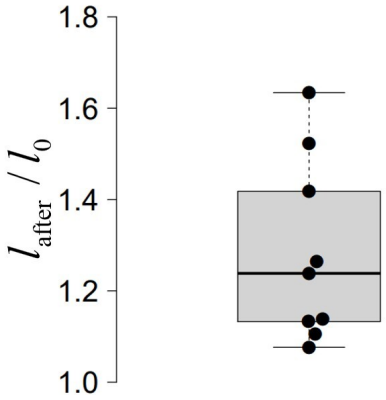

Fig. S4. Ratio between the initial middle junction length and its length after *direct push* manipulation.

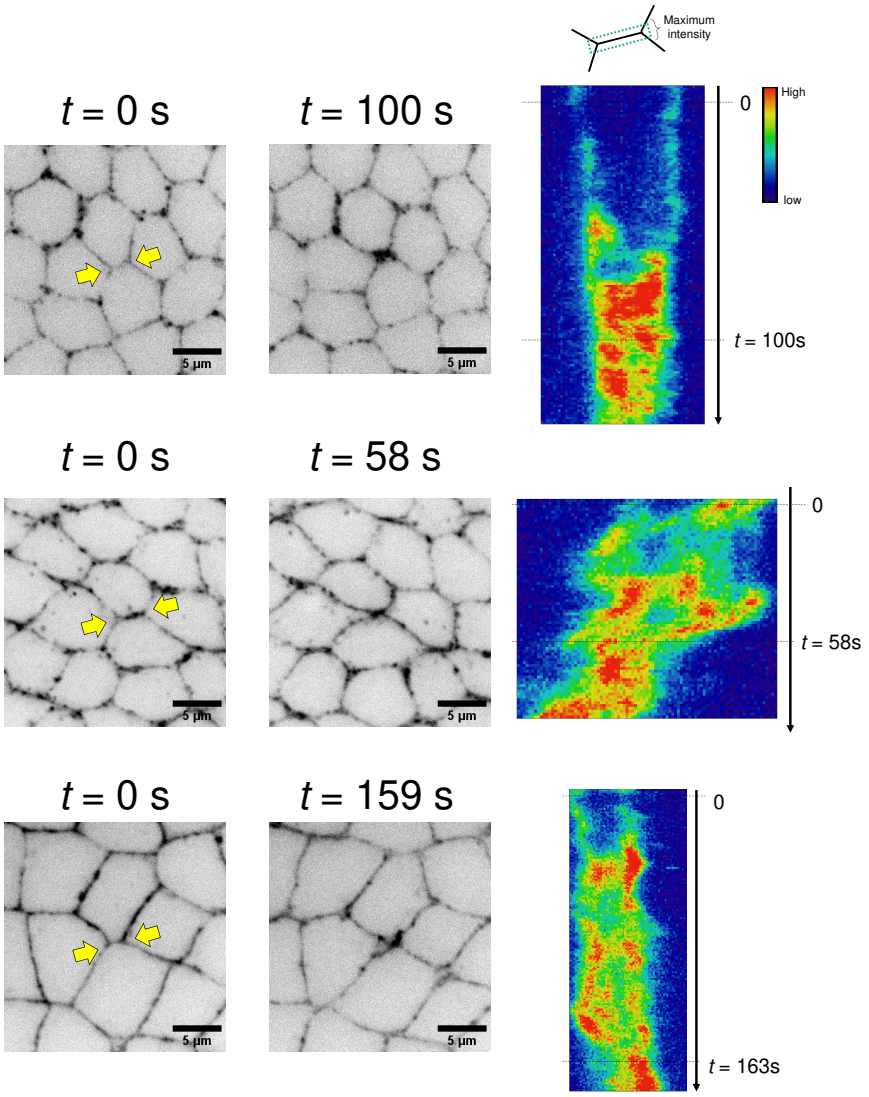

Fig. S5. F-actin response to *direct push*. F-actin (Utrophin::GFP, inverted contrast) at the onset of *direct push* experiment leading to junction shrinkage (left images). Scale bar: 5 μm. Corresponding kymographs along the junctions shrinking under *direct push*, showing accumulation of F-actin over time (right images).

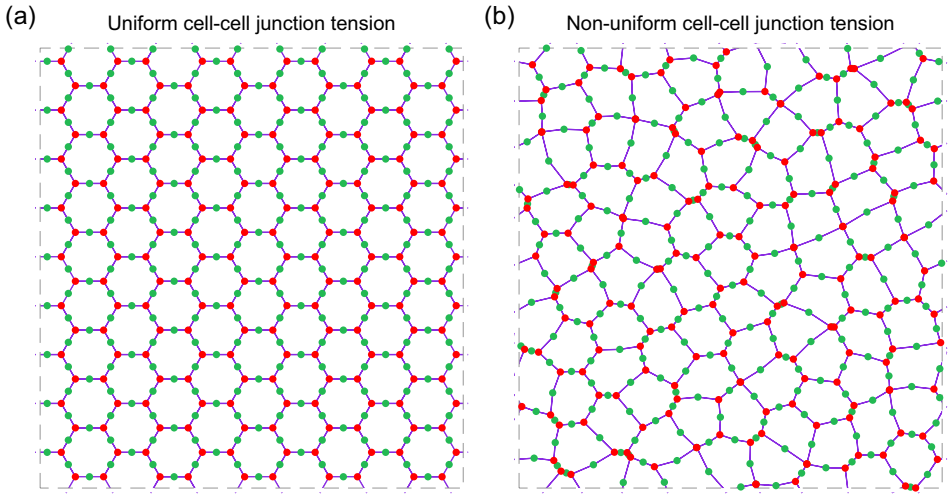

Fig. S6. Schematic of an epithelial vertex model. Shown here are two typical cell sheet patterns with different variation σ_T of cell-cell junction tension. Tricellular junctions are marked as red; while middle vertices are marked as green. (a) Uniform cell–cell junction tension with $\tilde{\sigma}_T = 0$. (b) Non-uniform cell–cell junction tension with $\tilde{\sigma}_T = 0.05$. For other parameter values, see Table S1.

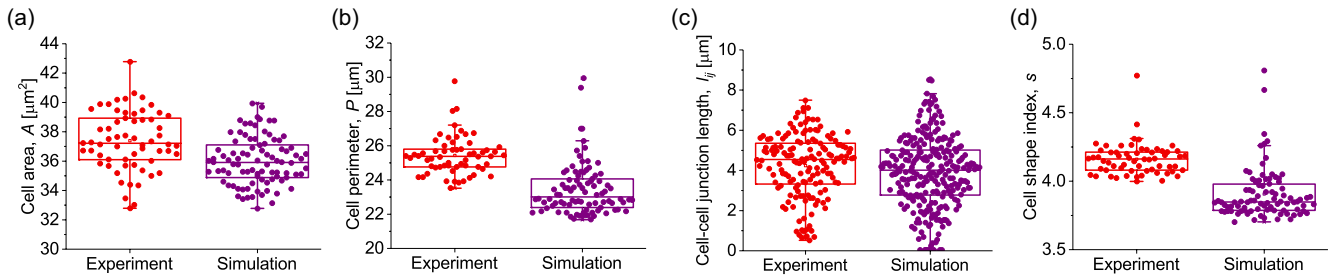

Fig. S7. Two-by-two comparison of cellular configuration distribution in experiments (red) and simulations (magenta): (a) cell area A; (b) cell perimeter P; (c) cell–cell junction length l_{ij}; (d) cell shape index $s = P/\sqrt{A}$. Parameters defined Table S1.

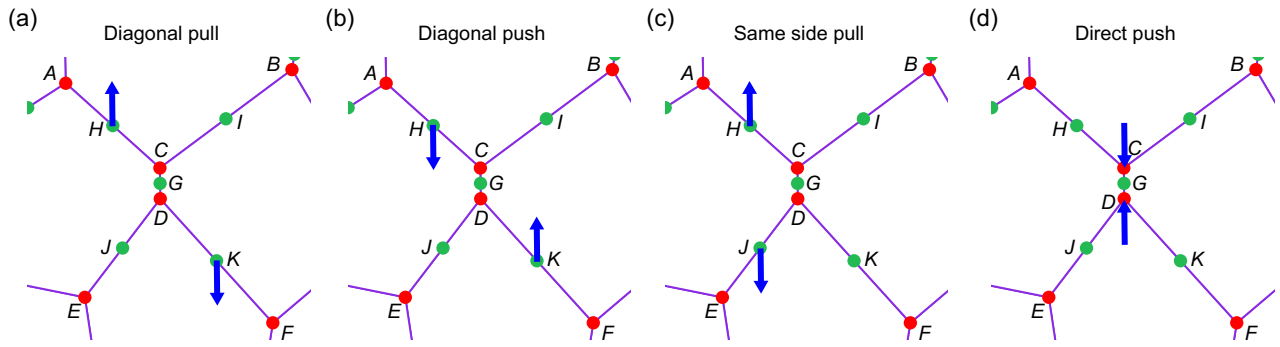

Fig. S8. Schematic of applying locally pulling/pushing forces in simulations. (a) *Diagonal pull* case, where the pulling forces are applied at vertices H and K in opposite directions (parallel to the junction $C - D$ initially) according to our optical trap model, see Eq. (2). (b) *Diagonal push* case, where the pushing forces are applied at vertices H and K in opposite directions (parallel to the junction $C - D$ initially). (c) *Same side pull* case, where the pulling forces are applied at vertices H and J in opposite directions (parallel to the junction $C - D$ initially). (d) *Direct push* case, where the pushing forces are applied at vertices C and D in opposite directions (parallel to the junction $C - D$ initially).

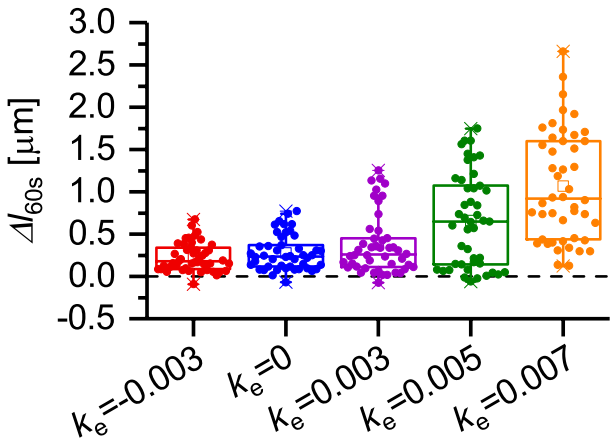

Fig. S9. Comparison of the middle junction elongation in the Model B simulations ($k_{\mathrm{c}} = 0$ and $T_m = 0$) of *diagonal pull*, for different values of k_{e}. Other parameters are defined in Table S1.

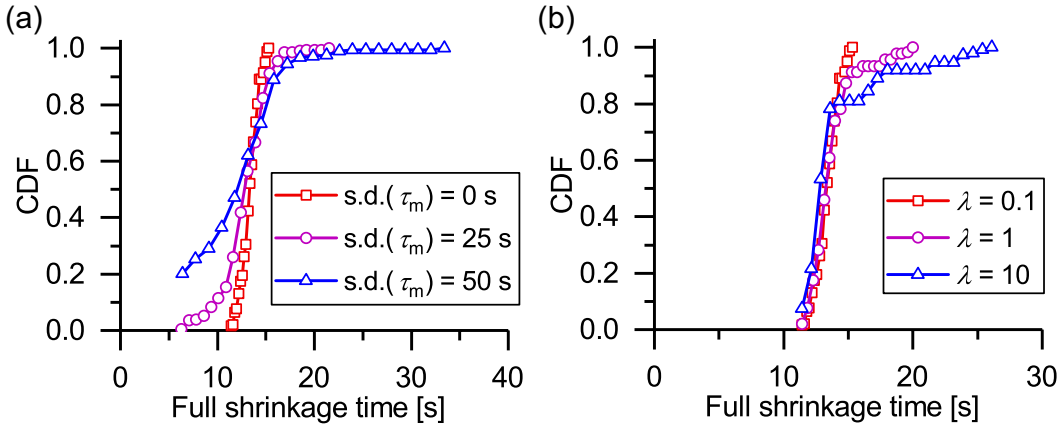

Fig. S10. Cumulative density function (CDF) of full-junction shrinkage time $t_{\mathrm{shrinkage}}$ in *direct push* simulations using the Model D, where the myosin accumulation is implemented using the standard exponential memory kernel, i.e. $\mathrm{Eq.}\ (8)$, with Gaussian-distributed characteristic time blur of the Myosin–II τ_m, with mean $\langle \tau_m \rangle$ and standard deviation $\mathrm{s.d.}(\tau_m)$. (a) CDF for $\langle \tau_m \rangle = 50$ s and varied $\mathrm{s.d.}(\tau_m)$ values (red: $\mathrm{s.d.}(\tau_m) = 0$, magenta: $\mathrm{s.d.}(\tau_m) = 25$ s; blue: $\mathrm{s.d.}(\tau_m) = 50$ s); here the smoothness of the activation function (see $\mathrm{Eq.}\ (7)$) is set at $\lambda = 0.1$. Both the values of $\langle \tau_d \rangle$ and $\mathrm{s.d.}(\tau_d)$ given here are those before truncation of the Gaussian distribution. (b) CDF for varied smoothness of the activation function λ values (red: $\lambda = 0.1$; magenta: $\lambda = 1$; blue: $\lambda = 10$), with fixed $\tau_m = 50$ s. Parameters: $\Delta_\varepsilon = 0.05$ and other parameter values are defined in Table S1.

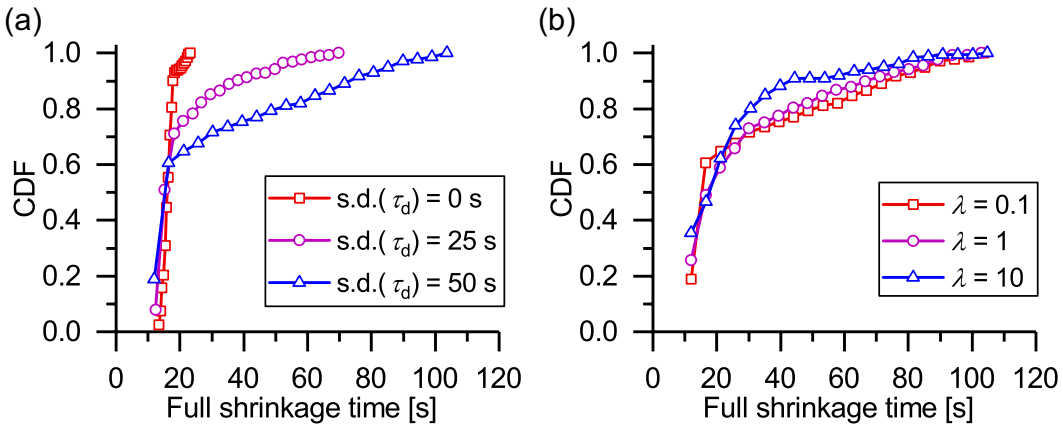

Fig. S11. Cumulative density function (CDF) of full-junction shrinkage time $t_{\mathrm{shrinkage}}$ in *direct push* simulations using the Model D, where the myosin accumulation is implemented using $\mathrm{Eq.}\ (9)$, with Gaussian-distributed time delays τ_d. (a) CDF with a mean time delay $\langle \tau_d \rangle = 50$s and three values of the time delay standard deviations values (red: $\mathrm{s.d.}(\tau_d) = 0$, magenta: $\mathrm{s.d.}(\tau_d) = 25$s; blue: $\mathrm{s.d.}(\tau_d) = 50$s); here the smoothness of the activation function (see $\mathrm{Eq.}\ (7)$) is set at $\lambda = 0.1$. Both the values of $\langle \tau_d \rangle$ and $\mathrm{s.d.}(\tau_d)$ given here are those before truncation of the Gaussian distribution. (b) CDF for varied smoothness of the activation function values (red: $\lambda = 0.1$; magenta: $\lambda = 1$; blue: $\lambda = 10$), with fixed time-delay mean $\langle \tau_d \rangle = 50$ s and standard deviation $\mathrm{s.d.}(\tau_d) = 50$ s. Parameters: $\Delta_\varepsilon = 0.05$ and other parameter values are defined in Table S1.

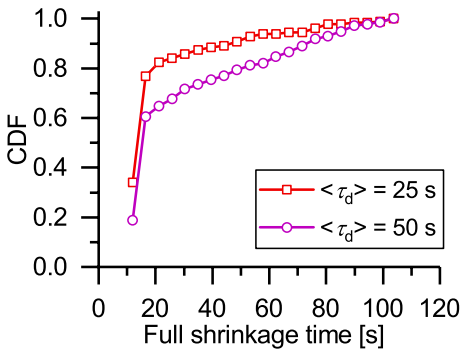

Fig. S12. Cumulative density function (CDF) of full-junction shrinkage time $t_{\mathrm{shrinkage}}$ in *direct push* simulations using the Model D, where the myosin accumulation is implemented using $\mathrm{Eq.}\ (9)$, with Gaussian-distributed time delays τ_d, of a mean value, $\langle \tau_d \rangle$, and a standard deviation value, $\mathrm{s.d.}(\tau_d)$. CDF with a standard deviation of time delay, $\mathrm{s.d.}(\tau_d) = 50$ s and two values of the mean time delay (red: $\langle \tau_d \rangle = 25$ s, magenta: $\langle \tau_d \rangle = 50$s). Both the values of $\langle \tau_d \rangle$ and $\mathrm{s.d.}(\tau_d)$ given here are those before truncation of the Gaussian distribution. Other parameter values are defined in Table S1.

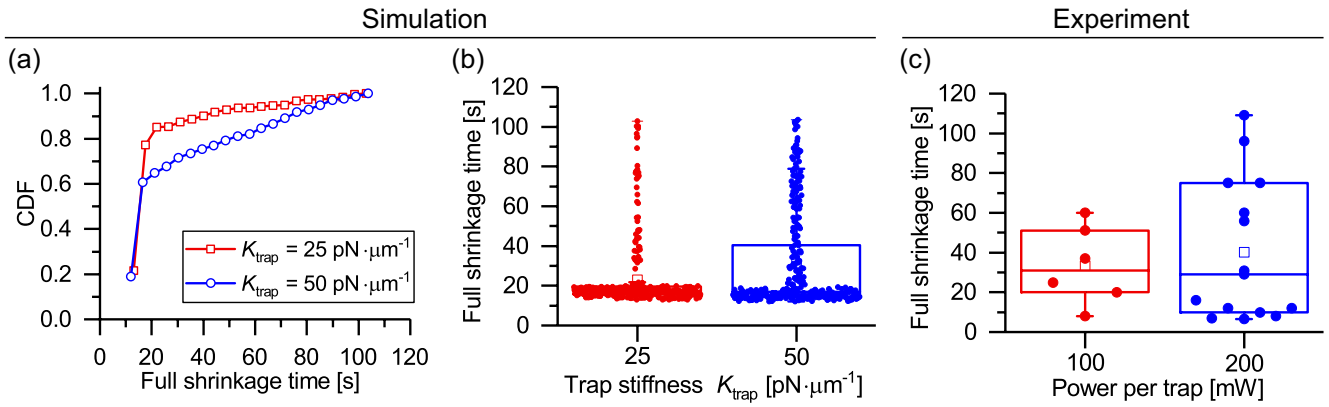

Fig. S13. (a, b) Simulations of the *direct push* case using the Model D, where the myosin accumulation is implemented using Eq. (9). (a) Cumulative density function (CDF) of full-junction shrinkage time $t_{\mathrm{shrinkage}}$, for different values of K_{trap}. (b) Scatter plot of the full-junction shrinkage time $t_{\mathrm{shrinkage}}$, for different values of K_{trap}. Number of data: $n_{25\ \mathrm{pN}\cdot\mu\mathrm{m}^{-1}} = 316$ and $n_{50\ \mathrm{pN}\cdot\mu\mathrm{m}^{-1}} = 313$. Specifically, for $K_{\mathrm{trap}} = 25\ \mathrm{pN}\cdot\mu\mathrm{m}^{-1}$, $t_{\mathrm{shrinkage}} = 23 \pm 17\ \mathrm{s}$; while for $K_{\mathrm{trap}} = 50\ \mathrm{pN}\cdot\mu\mathrm{m}^{-1}$, $t_{\mathrm{shrinkage}} = 31 \pm 25\ \mathrm{s}$. Parameters: $\langle\tau_d\rangle = 50\ \mathrm{s}$ and $\mathrm{s.d.}(\tau_d) = 50\ \mathrm{s}$; other parameter values are defined in Table S1. Both the values of $\langle\tau_d\rangle$ and $\mathrm{s.d.}(\tau_d)$ given here are those before truncation of the Gaussian distribution. (c) Experimental result: scatter plot of the full-junction shrinkage time $t_{\mathrm{shrinkage}}$, for different values of power per trap. Number of data: $n_{100\ \mathrm{mW}} = 6$ and $n_{200\ \mathrm{mW}} = 15$. Simulation parameters are defined in Table S1.

Table S1. List of parameter values used in the simulations (Model D).

Parameter	Description	Value	Dimensionless value
K_A	Cell area stiffness	$10^6\ \mathrm{N}\cdot\mathrm{m}^{-3}$ (9)	1
A_0	Preferred cell area	$36\ \mu\mathrm{m}^2$	1
μ_T	Average cell junctional tension	$44\ \mathrm{pN}$ (2)	0.2
σ_T	Standard derivation of cell junctional tension	$11\ \mathrm{pN}$	0.05
Δ_{trap}	Displacement of the optical trap	$1.2\ \mu\mathrm{m}$	0.2
K_{trap}	Stiffness of the optical trap	$50\ \mathrm{pN}\cdot\mu\mathrm{m}^{-1}$ (2)	1.4
k_L	Remodeling rate of rest length	$0.04\ \mathrm{s}^{-1}$	0.04
k_{e}	Tension remodeling rate under extension	$0.18\ \mathrm{pN}\cdot\mu\mathrm{m}^{-1}\cdot\mathrm{s}^{-1}$	0.005
k_{c}	Tension remodeling rate under contraction	$-0.108\ \mathrm{pN}\cdot\mu\mathrm{m}^{-1}\cdot\mathrm{s}^{-1}$	-0.003
$\varepsilon_{\mathrm{cr}}$	Strain threshold for tension remodeling	0.1	0.1
$\dot{\varepsilon}_{\mathrm{cr}}^{(\mathrm{myo})}$	Strain rate threshold for myosin recruitment at cell–cell junctions	$-0.05\ \mathrm{s}^{-1}$	-0.05
T_m	Tension magnitude induced by myosin recruitment at cell–cell junctions	$270\ \mathrm{pN}$	1.25
$\langle\tau_d\rangle;\mathrm{s.d.}(\tau_d)$	Mean time and standard deviation in the delay to the myosin recruitment at cell–cell junctions	$25\ \mathrm{s};\ 50\ \mathrm{s}$	$25;\ 50$
τ_m	Blur in the myosin signal	$50\ \mathrm{s}$	50
$\lambda;\Delta_\epsilon$	Smoothness of the myosin recruitment activation profile	$0.1;\ 0.05\ \mathrm{s}^{-1}$	$0.1;\ 0.05$
Δt	Simulation time step	$0.01\ \mathrm{s}$	0.01
$\ell=\sqrt{A_0}$	Length scale	$6\ \mu\mathrm{m}$	1
$\tau=\gamma/(K_A A_0)$	Time scale	$1\ \mathrm{s}$	1
$\sigma=K_A A_0$	Stress scale	$36\ \mathrm{pN}\cdot\mu\mathrm{m}^{-1}$	1

References

1. EJ Peterman, F Gittes, CF Schmidt, Laser-induced heating in optical traps. *Biophys. journal* **84**, 1308–1316 (2003).
2. K Bambardekar, R Clément, O Blanc, C Chardès, PF Lenne, Direct laser manipulation reveals the mechanics of cell contacts in vivo. *Proc. Natl. Acad. Sci. United States Am.* **112**, 1416–1421 (2015).
3. R Farhadifar, JC Röper, B Algouy, S Eaton, F Jülicher, The influence of cell mechanics, cell–cell interactions, and proliferation on epithelial packing. *Curr. Biol.* **17**, 2095–2104 (2007).
4. AG Fletcher, M Osterfield, RE Baker, SY Shvartsman, Vertex models of epithelial morphogenesis. *Biophys. J.* **106**, 2291–2304 (2014).
5. D Bi, J Lopez, J Schwarz, ML Manning, A density-independent rigidity transition in biological tissues. *Nat. Phys.* **11**, 1074–1079 (2015).
6. SZ Lin, S Ye, GK Xu, B Li, XQ Feng, Dynamic migration modes of collective cells. *Biophys. J.* **115**, 1826–1835 (2018).
7. MF Staddon, KE Cavanaugh, EM Munro, ML Gardel, S Banerjee, Mechanosensitive junction remodeling promotes robust epithelial morphogenesis. *Biophys. J.* **117**, 1739–1750 (2019).
8. HV Prentice-Mott, et al., Directional memory arises from long-lived cytoskeletal asymmetries in polarized chemotactic cells. *Proc. Natl. Acad. Sci. United States Am.* **113**, 1267–72 (2016).
9. PP Girard, EA Cavalcanti-Adam, R Kemkemer, JP Spatz, Cellular chemomechanics at interfaces: sensing, integration and response. *Soft Matter* **3**, 307–326 (2007).

4. Movie captions

Movie S1 (separate file). Diagonal pull manipulation
A movie of *diagonal pull* manipulation, which corresponds to Fig. 1B in the main text (E-cad::GFP). The length change at 60 s post-manipulation is $\Delta l_{60s} = 1.13$ μm. Total duration is 70 s (10 times fast forward). Red circles are the two positions of laser focus. Scale bar: 5 μm.

Movie S2 (separate file). Simulation of diagonal pull manipulation
A movie of numerical simulation of a *diagonal pull* manipulation using model D as described in the main text.

Movie S3 (separate file). Fast shrinkage in *direct push* manipulation
A movie of *direct push* manipulation, which corresponds to Fig. 3B (left) in the main text (E-cad::GFP). The junction was shrunk fast (7 s) after applying optical forces. Scale bar: 5 μm.

Movie S4 (separate file). Slow shrinkage in *direct push* manipulation
A movie of *direct push* manipulation which is corresponding to Fig. 3B (right) in the main text (E-cad::GFP). The junction was slowly shrunk (109 s) after force application. Scale bar: 5 μm.

Movie S5 (separate file). *direct push* manipulation for a Rock-inhibited tissue
A movie of *direct push* manipulation for a Rock-inhibited tissue, which corresponds to Fig. 4A in the main text (E-cad::GFP). The junction was not shrunk and escaped from optical manipulation. Scale bar: 5 μm.

Movie S6 (separate file). Myosin II response during junction shrinkage
A movie of *direct push* manipulation, which corresponds to Fig. 4C in the main text (Sqh::GFP, inverted contrast). Scale bar: 5 μm.

Movie S7 (separate file). F-actin response during junction shrinkage
A movie of *direct push* manipulation which is corresponding to Fig. S5 (Utrophin::GFP, inverted contrast). Scale bar: 5 μm.